Article

Cell Reports

Reduced Insulin/IGF-1 Signaling Restores the Dynamic Properties of Key Stress Granule Proteins during Aging

Graphical Abstract

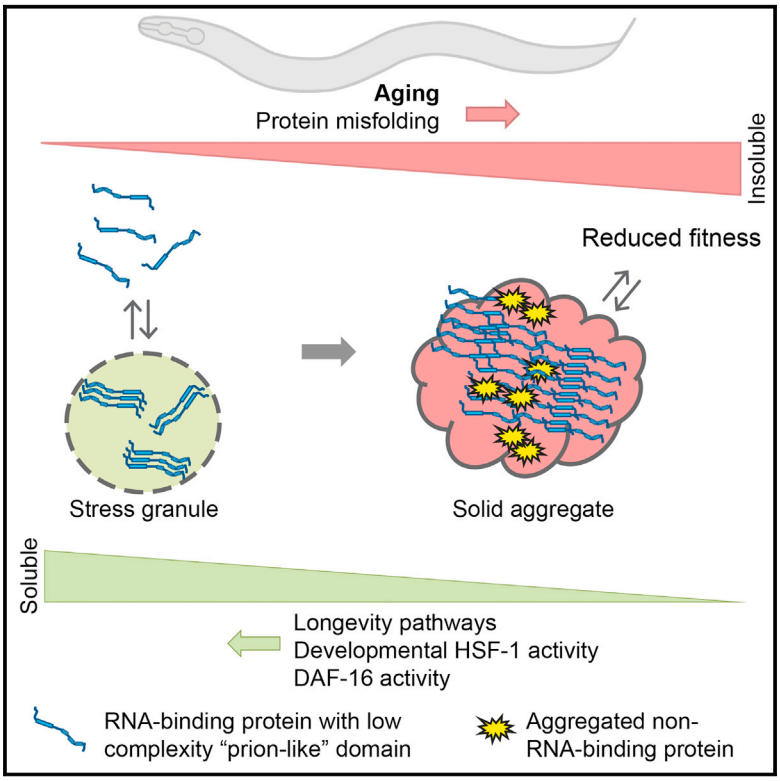

Authors

Marie C. Lechler, Emily D. Crawford, Nicole Groh, ..., Jonathan C. Trinidad, Alma L. Burlingame, Della C. David

Correspondence

della.david@dzne.de

In Brief

Lechler et al. show that RNA-binding proteins (RBPs) including stress granule proteins are prone to aggregate with age in *C. elegans*. Aggregation of stress granule RBPs with "prion-like" domains is associated with reduced fitness. Their aggregation is prevented by longevity pathways and promoted by the aggregation of other misfolded proteins.

Highlights

- RNA-binding proteins (RBPs) with "prion-like" domains form solid aggregates with age
- Reduced *daf-2* signaling preferentially prevents insolubility of RNA granule proteins
- Co-aggregation with other misfolded proteins promotes stress granule RBP aggregation
- Aggregation of key stress-granule-related RBPs is associated with impaired health

Accession Numbers

PXD003451

Lechler et al., 2017, Cell Reports *18*, 454–467
January 10, 2017
http://dx.doi.org/10.1016/j.celrep.2016.12.033

OPEN ACCESS
CellPress

Cell Reports
Article

Reduced Insulin/IGF-1 Signaling Restores the Dynamic Properties of Key Stress Granule Proteins during Aging

Marie C. Lechler,[1,2] Emily D. Crawford,[1,5] Nicole Groh,[1,2] Katja Widmaier,[1] Raimund Jung,[1] Janine Kirstein,[3] Jonathan C. Trinidad,[4,6] Alma L. Burlingame,[4] and Della C. David[1,7,*]

[1]German Center for Neurodegenerative Diseases, 72076 Tübingen, Germany
[2]Graduate Training Centre of Neuroscience, 72074 Tübingen, Germany
[3]Leibniz-Institut für Molekulare Pharmakologie im Forschungsverbund Berlin, 13125 Berlin, Germany
[4]Mass Spectrometry Facility, Department of Pharmaceutical Chemistry, University of California, San Francisco, San Francisco, CA 94158, USA
[5]Present address: Department of Biochemistry and Biophysics, University of California, San Francisco, San Francisco, CA 94158, USA
[6]Present address: Department of Chemistry, Indiana University, Bloomington, IN 47405, USA
[7]Lead Contact
*Correspondence: della.david@dzne.de
http://dx.doi.org/10.1016/j.celrep.2016.12.033

SUMMARY

Low-complexity "prion-like" domains in key RNA-binding proteins (RBPs) mediate the reversible assembly of RNA granules. Individual RBPs harboring these domains have been linked to specific neurodegenerative diseases. Although their aggregation in neurodegeneration has been extensively characterized, it remains unknown how the process of aging disturbs RBP dynamics. We show that a wide variety of RNA granule components, including stress granule proteins, become highly insoluble with age in *C. elegans* and that reduced insulin/insulin-like growth factor 1 (IGF-1) *daf-2* receptor signaling efficiently prevents their aggregation. Importantly, stress-granule-related RBP aggregates are associated with reduced fitness. We show that heat shock transcription factor 1 (HSF-1) is a main regulator of stress-granule-related RBP aggregation in both young and aged animals. During aging, increasing DAF-16 activity restores dynamic stress-granule-related RBPs, partly by decreasing the buildup of other misfolded proteins that seed RBP aggregation. Longevity-associated mechanisms found to maintain dynamic RBPs during aging could be relevant for neurodegenerative diseases.

INTRODUCTION

Young, healthy organisms strive to maintain their proteome in a functional state through the tight control of rates of protein synthesis, folding, and degradation. Extensive quality-control systems are set up throughout the cell to prevent and manage protein damage. As the organism ages, these control mechanisms become less efficient, leading to a disruption in protein homeostasis (Balch et al., 2008; David, 2012). Aging is the main risk factor for a variety of neurodegenerative diseases where specific proteins accumulate as pathological aggregates. Recently, there has been considerable interest in investigating widespread protein aggregation in the absence of disease. Multiple studies have demonstrated that several hundred proteins become highly detergent-insoluble in aged animals (Ayyadevara et al., 2016; David, 2012; David et al., 2010; Demontis and Perrimon, 2010; Reis-Rodrigues et al., 2012; Tanase et al., 2016; Walther et al., 2015). Computational analysis of the insoluble proteome indicates an overrepresentation of proteins with functional and structural similarities (David et al., 2010). The examination of some of these proteins in vivo reveals their assembly into large "solid" aggregates with age similar to those formed in the context of disease. The discovery of endogenous age-dependent protein aggregation in model organisms gives us the unprecedented opportunity to dissect the intrinsic cellular machineries responsible for preventing protein aggregation without using ectopically expressed human disease-associated proteins. At this time, very little is known concerning the regulation of widespread protein insolubility with age and its consequences for the health of the organism. Interestingly, several studies show that protein insolubility is modified in long-lived animals with reduced insulin/insulin growth factor (IGF)-1 *daf-2* signaling, but it remains unclear to which extent (David et al., 2010; Demontis and Perrimon, 2010; Walther et al., 2015).

A growing number of familial and sporadic forms of neurodegenerative diseases show pathological inclusions caused by abnormal aggregation of RNA-binding proteins (RBPs). The first RBPs identified in these inclusions were TAR DNA binding protein of 43 kDa (TDP-43) and fused in sarcoma (FUS), associated with amyotrophic lateral sclerosis (ALS) and frontotemporal lobar degeneration (FTLD) (Arai et al., 2006; Neumann et al., 2009; Neumann et al., 2006). Since then additional RBPs such as TAF15, EWSR1, hnRNPA2B1, hnRNPA1,

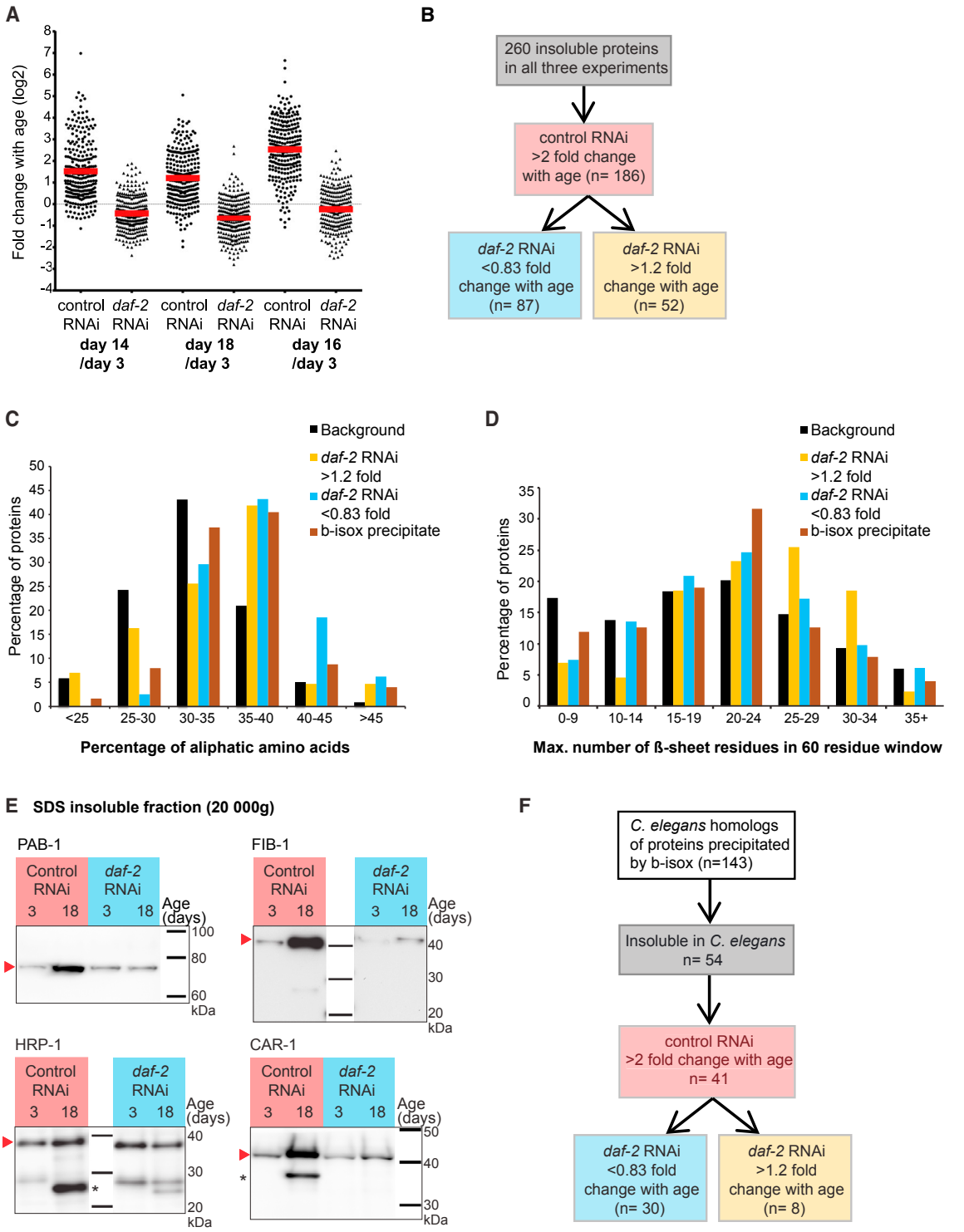

Figure 1. RNA Granule Components No Longer Aggregate in Long-Lived Animals with Reduced *daf-2* Signaling

(A) Distribution of fold changes with age in insolubility for 260 proteins (n = 3, biological replicates). Fold changes are measured by iTRAQ quantification.

(B) Flowchart describing the segregation of insolubility fold changes with age into different groups for analysis.

(C) Proteins with reduced aggregation in *daf-2* RNAi conditions and U2OS proteins precipitated by b-isox are enriched in aliphatic amino acids. Unequal variance t test: proteins aggregating more with age in long-lived animals (n = 43, >1.2-fold), p = 0.04; proteins aggregating less with age in long-lived animals (n = 81, <0.83-fold), p = 6.1E-15; proteins precipitated by b-isox (n = 126), p = 1.3E-9.

(legend continued on next page)

and hnRNPA3 have been associated with neurodegenerative diseases (Kim et al., 2013; Neumann et al., 2011). All of the known RBPs associated with dementia contain a low-complexity (LC) "prion-like" domain enriched in glycines and uncharged polar amino acids, and similar to the sequences driving yeast prion aggregation (Alberti et al., 2009; King et al., 2012). Mutations in this domain enhance pathology by accelerating aggregation (Johnson et al., 2009; Kim et al., 2013). LC prion-like domains are also present in key RBPs that mediate the assembly of RNA granules by liquid-liquid phase separation (Lin et al., 2015; Molliex et al., 2015; Murakami et al., 2015; Patel et al., 2015). Significantly, a small proportion of liquid droplets made by RBPs transform into solid aggregates over time in vitro (Lin et al., 2015; Molliex et al., 2015; Murakami et al., 2015; Patel et al., 2015). For clarity, we will use the term *aggregation* only when referring to the formation of non-dynamic RBP aggregates. An important question is whether the special assembly properties of RBPs puts them at risk of aggregating during aging in a multicellular organism and not just in the context of disease. Interestingly, several RBPs with LC prion-like domains were identified in the insoluble proteome of aged animals (David et al., 2010). Overall, it is imperative to know the causes and consequences of wild-type RBP aggregation during aging in order to fully understand RBP aggregation in neurodegenerative diseases. Furthermore, it is likely that the organism has evolved specific mechanisms to control liquid droplet protein aggregation.

In the current study, we chose to focus on key RBPs responsible for stress granule formation. Stress granules are a specific type of RNA granule that protect the cell by sequestering mRNA from the translational machinery during periods of stress. Importantly, stress granule proteins are often found to co-localize with pathological inclusions of TDP-43 and FUS (Bentmann et al., 2013; Li et al., 2013). Whether these stress granule proteins are innocent bystanders transiently interacting with TDP-43 and FUS or whether they co-aggregate and accelerate disease-associated RBP aggregation remains intensely debated (Bentmann et al., 2013; Li et al., 2013).

We show that key stress-granule-related RBPs (sgRBPs) accumulate in aberrant stress granule-like puncta and in large solid aggregates in aged *C. elegans*. Proteomic analysis revealed that long-lived animals with reduced *daf-2* signaling preferentially abrogate the insolubility of RNA granule components. Importantly, sgRBP aggregates are associated with reduced animal size, motility, and lifespan. We show that sgRBP aggregation is triggered at an earlier age by their co-aggregation with other misfolded proteins, a process that is prevented by DAF-16 in *daf-2* mutants. In addition, the proteostasis network established by heat shock transcription factor 1 (HSF-1) during development is required to maintain dynamic stress granule proteins throughout the animal's life.

RESULTS

Long-Lived Animals with Reduced *daf-2* Signaling Prevent Widespread Protein Insolubility with Age

To identify and quantify changes in aggregation-prone proteins in animals with reduced *daf-2* signaling, we performed an in-depth proteomic analysis of the insoluble proteome from both control and long-lived animals (Figure 1A; Table S1). Because protein misfolding and aggregation is highly abundant in aged *C. elegans* gonads and masks changes in other somatic tissues (David et al., 2010; Goudeau and Aguilaniu, 2010; Zimmerman et al., 2015), we used a gonad-less mutant to focus our analysis on protein insolubility in non-reproductive tissues. We isolated large aggregates that are pelleted by low centrifugal forces (20,000 × *g*) and insoluble in 0.5% SDS. In three biological replicates, we identified 260 insoluble proteins, of which 186 were highly prone to aggregate with age in control animals (Figure 1B). The strong correlations between the control replicates ($r = 0.77$, $r = 0.85$, and $r = 0.67$) and long-lived replicates ($r = 0.87$, $r = 0.86$. and $r = 0.82$) attest to the quality of the quantification and experimental reproducibility (Figures S1A and S1B). None of these insoluble proteins was more prone to aggregate with age in the long-lived animals as compared with controls. These results are consistent with previous observations (David et al., 2010; Demontis and Perrimon, 2010). Surprisingly, a recent proteomic study showed that endogenous protein insolubility is higher in *daf-2* mutants than in wild-type animals (Walther et al., 2015). To account for procedural differences, we performed the extraction following the less stringent extraction protocol from Walther et al. (2015). By omitting SDS and using ultracentrifugation at 500,000 × *g*, Walther et al. analyzed highly insoluble large aggregates (as in this study), as well as smaller and more soluble aggregates. However, we did not observe a general change in the action of *daf-2* signaling on protein insolubility with age after using the less stringent extraction protocol (Figure S1C). Next, we asked whether the inconsistencies between the studies could be related to protein aggregation in the gonad and indeed, we found that long-lived animals with gonads have proportionally more insoluble proteins compared with wild-type animals with gonads (Figure S1D). These results suggest that aggregation in the gonad masks the protective effect of reduced *daf-2* signaling in somatic tissues. Importantly, we confirmed this protective action of reduced *daf-2* signaling with several candidates (see below).

Taken together, these data demonstrate that reduced *daf-2* signaling promotes protein solubility in most tissues with age.

(D) Proteins that aggregate in both control and *daf-2* RNAi conditions are enriched in extended stretches of β-sheet propensity. Unequal variance t test: proteins aggregating more with age in long-lived animals (n = 43, >1.2-fold), p = 0.002; proteins aggregating less with age in long-lived animals (n = 81, <0.83-fold), p = 0.09; proteins precipitated by b-isox (n = 126), p = 0.6.

(E) Large SDS-insoluble aggregates precipitated by 20,000 × *g*. Immunoblots detecting RBPs PAB-1, FIB-1, HRP-1 (unspecific band noted by asterisk), and CAR-1 (truncated band marked by asterisk). Relevant protein bands are indicated by red arrow.

(F) Flowchart showing a high overlap between proteins precipitated by b-isox and aggregation-prone proteins in *C. elegans*, in particular those no longer aggregating in *daf-2(–)* conditions.

See also Figures S1, S2, and S3 and Tables S1, S2, S3, and S4.

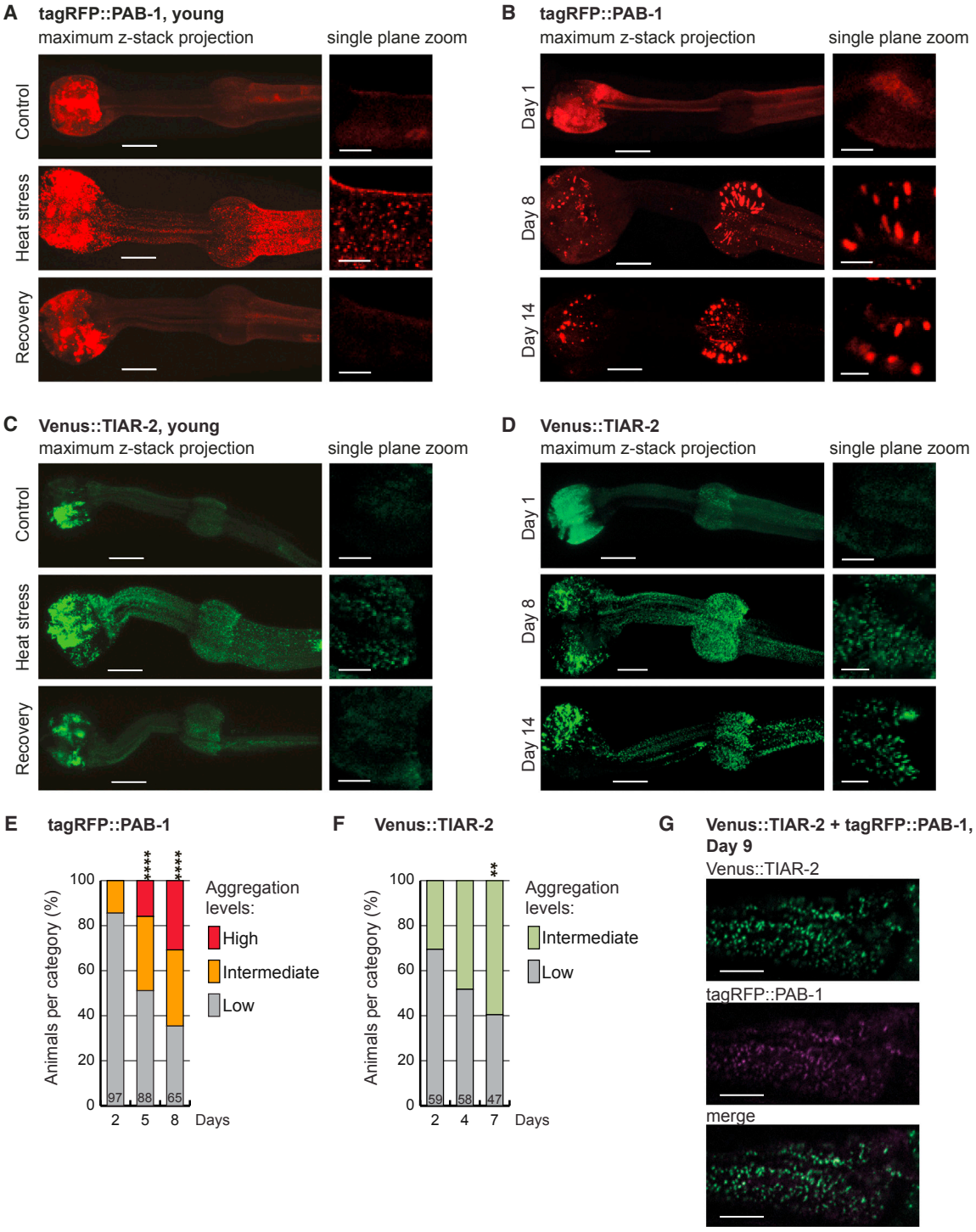

Figure 2. Stress-Granule-Related RBPs PAB-1 and TIAR-2 Aggregate with Age in *C. elegans*

(A) tagRFP::PAB-1 expressed in the pharyngeal muscles forms stress granules upon heat stress (2 hr, 32°C) on day 1 of adulthood. No stress granules are visible after recovery (+24 hr). Scale bars: z stack projection, 15 μm; single-plane insets, 5 μm.

(B) tagRFP::PAB-1 distribution changes from a diffuse pattern in young animals to a punctate pattern in aged worms. Scale bars: z stack projection, 15 μm; single-plane insets, 5 μm.

(C) Venus::TIAR-2 expressed in the pharyngeal muscles forms stress granules upon heat stress (2 hr, 32°C) on day 1 of adulthood. No stress granules are visible after recovery (+24 hr). Scale bars: z stack projection, 15 μm; single-plane insets, 5 μm.

(D) Venus::TIAR-2 accumulates mainly in stress-granule-like puncta with age. Scale bars: z stack projection, 15 μm; single-plane insets, 5 μm.

(legend continued on next page)

Reduced *daf-2* Signaling Preferentially Abrogates the Insolubility of RNA Granule Components

To investigate specifically changes in insolubility regulated by reduced *daf-2* signaling, we sorted proteins prone to aggregate with age in control animals (>2-fold) by their fold change in insolubility with age in the long-lived conditions. We restricted our analysis to 87 proteins that aggregated less with age (<0.83-fold) and 52 proteins that continued to aggregate with age (>1.2-fold) in the long-lived animals (Figure 1B; Table S1). Previous bioinformatics analysis of aggregation-prone proteins revealed an enrichment in both β-sheet propensity and aliphatic amino acids (David et al., 2010). A similar enrichment in the whole insoluble proteome was identified in this study (Figures S1E and S1F). Intriguingly, when examining the two groups of insoluble proteins that were differentially regulated by reduced *daf-2* signaling, we found a segregation of the two properties. Proteins with abrogated aggregation with the *daf-2* RNAi treatment were highly enriched in aliphatic amino acids, in particular alanine, glycine, and valines, but not in β sheets (Figures 1C, 1D, and S1G). Conversely, proteins that still aggregate in the *daf-2(−)* condition had a significant propensity to form β sheets but were only modestly enriched in aliphatic amino acids (Figures 1C and 1D).

Next, we searched for functional differences between the two groups differentially regulated by reduced *daf-2* signaling. Strikingly, ribosomal proteins and RNA granule components, including stress granule and P-granule RBPs, were highly overrepresented among the proteins that were prevented from aggregating with age in the long-lived animals (Tables S2A and S3). Conversely, chaperones and vitellogenin yolk proteins were overrepresented among proteins that were still prone to aggregate with age in *daf-2(−)* conditions (Table S2B). Among the RBPs, four are predicted to have LC prion-like domains (Alberti et al., 2009): PAB-1, FIB-1, HRP-1, and CAR-1 (Figure S2A). By western blot, we confirmed that reduced *daf-2* signaling abrogated their aggregation with age (Figures 1E and S2B). In addition, we evaluated two proteins without RNA-binding or LC prion-like domains, PAR-5 and DAF-21, quantified by mass spectrometry as more insoluble with age in both control and long-lived animals. We confirmed that PAR-5 and DAF-21 continued to aggregate with age in long-lived animals (by >7-fold and 10-fold, respectively), albeit to a reduced extent compared with controls (Figure S2C). Of note, changes in aggregation were not correlated with changes in total protein levels (Figure S3).

A previous study found that the chemical b-isox exclusively causes RNA granules to precipitate out from whole-cell lysates by inducing their assembly into a hydrogel (Han et al., 2012; Kato et al., 2012). Proteins precipitated by b-isox were also enriched in aliphatic amino acids (in particular glycine and to a lesser extent alanine and valine) and not in the propensity to form β sheets (Figures 1C, 1D, and S1G). We checked for proteins in common with our study and found a very significant overlap between proteins precipitated by b-isox and proteins no longer aggregating in the long-lived conditions (Figure 1F; Table S4).

Together, these results indicate that different types of RNA granule components including key RBPs responsible for their assembly become insoluble with age, and long-lived animals with reduced *daf-2* signaling are highly successful in preventing their aggregation. Interestingly, higher levels of aliphatic amino acids in RNA granule components could help their assembly and/or drive their age-dependent aggregation.

Key Stress Granule Proteins PAB-1 and TIAR-2 Form Solid Aggregates in Aged *C. elegans*

To investigate further the aggregation of key RBPs with LC prion-like domains and to understand the mechanisms involved, we generated *C. elegans* strains expressing PAB-1 and TIAR-2 in the pharyngeal muscles, fused to fluorescent tags. PAB-1 and TIAR-2 are the *C. elegans* homologs of human polyadenylate-binding protein 1 (PABP-1) and T-cell-restricted intracellular antigen-1 (TIA-1), two prominent RBPs that localize to stress granules and are also minor components of pathological inclusions that occur in ALS and FLTD (Bentmann et al., 2012). Both of these RBPs harbor LC prion-like domains (Figure S2A) (Alberti et al., 2009).

Exposing cells to stressors such as heat induces RBPs with LC prion-like domains to form liquid droplets (Molliex et al., 2015; Patel et al., 2015). Similarly, heat shock in *C. elegans* caused PAB-1 and TIAR-2 to form stress granules (Figures 2A and 2C; Figure S4A) (Murakami et al., 2012; Rousakis et al., 2014). When co-expressed, PAB-1 and TIAR-2 localized to the same stress granules (Figure S4B). Consistent with the dynamic nature of stress granules, these puncta were no longer observed 24 hr after the heat shock (Figures 2A and 2C). Using antibodies, we observed a similar change in pattern with endogenous PAB-1, indicating the effect is not merely due to overexpression or the fluorescent tag (Figure S4C). As an additional control, we showed that kinase KIN-19, which is not an RBP and lacks a LC prion-like domain, does not localize to stress granules upon heat shock (Figure S4D).

With age, we observed a striking change in the distribution pattern of these key stress granule RBPs. Whereas the majority of PAB-1 and TIAR-2 proteins were diffusely localized in non-stressed young animals, we found that both stress granule components accumulated in distinct puncta in aged animals (Figures 2B and 2D; Figure S4F). This change was specific for PAB-1 and TIAR-2 as the fluorescent tags alone (Venus or tagRFP) remained diffuse with age (Figure S4E) (David et al., 2010). The results were not simply caused by overexpression because endogenous PAB-1 formed similar puncta with age, in the different head regions where it is natively expressed (Figure S4G). For both PAB-1 and TIAR-2, we observed a significant increase with

(E) Increased tagRFP::PAB-1 aggregation with age in a population of *C. elegans*. Day 5 or 8 versus day 2: ****$p < 0.0001$.
(F) Increased Venus::TIAR-2 aggregation with age in a population of *C. elegans*. Day 7 versus day 2: **$p < 0.01$.
(G) tagRFP::PAB-1 co-localizes with stress-granule-like Venus::TIAR-2 puncta in double-transgenic animals. Representative single-plane images. Scale bar, 7 μm.
See also Figure S4.

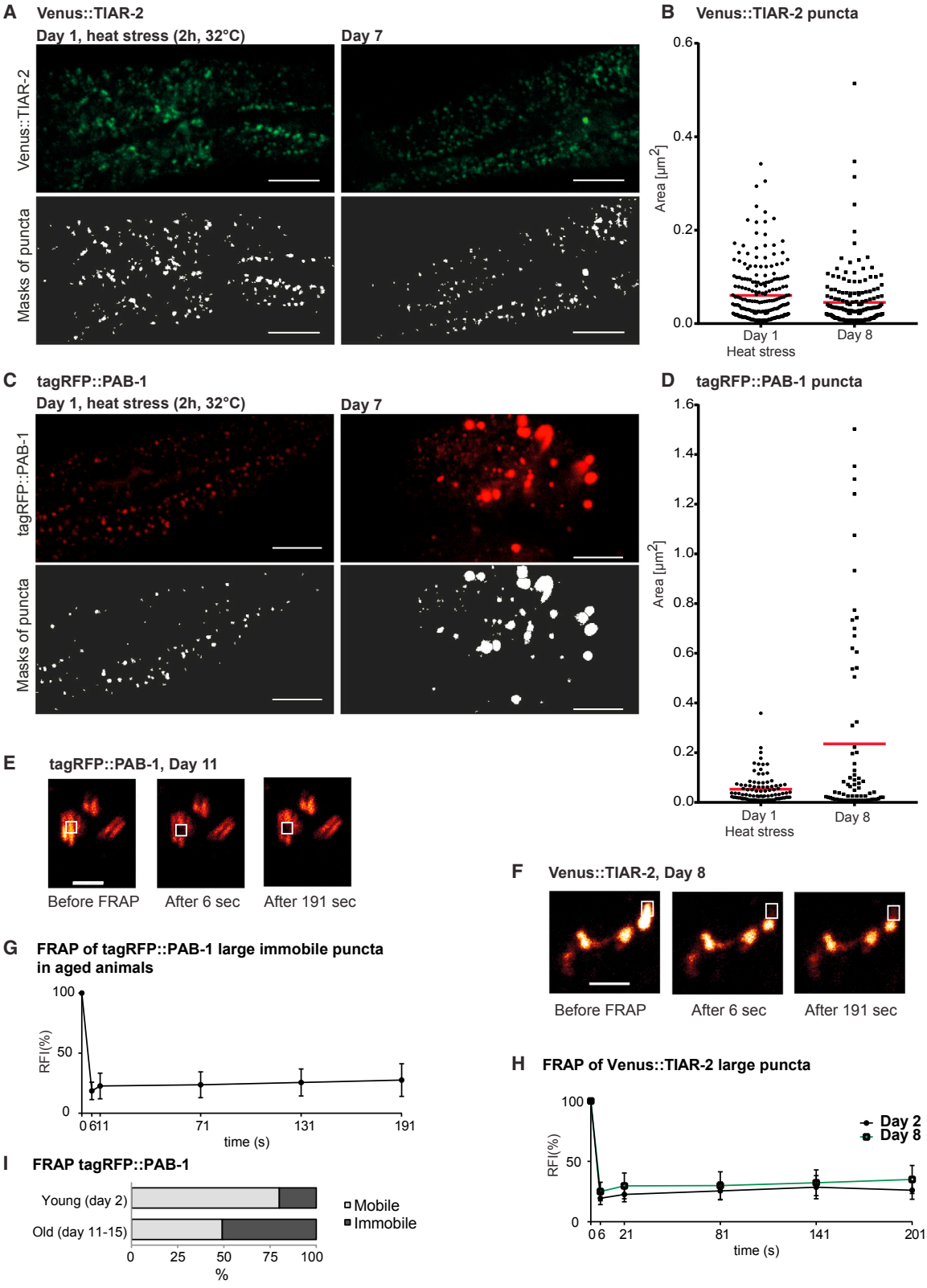

(legend on next page)

age in the number of worms with large puncta that are visible by low-magnification microscopy (Figures 2E and 2F; Figure S4H). Interestingly, imaging at high magnification revealed that TIAR-2 in aged animals was localized predominantly in small puncta highly reminiscent of stress granules assembled during heat shock, whereas PAB-1 accumulated to a greater extent in large puncta that were not normally observed upon heat shock in young animals (Figures 2B, 2D, single-plane insets, 3A, 3C, and 3D). Quantification confirmed that stress granules induced during heat shock and aberrant TIAR-2 stress granule-like puncta formed during aging had similar sizes (Figure 3B). Remarkably, when co-expressed, PAB-1 preferentially co-localized within TIAR-2-positive age-dependent stress-granule-like puncta (Figure 2G), suggesting that interactions between RBPs change their aggregation patterns.

A hallmark of protein aggregation associated with disease is the immobility of proteins within the aggregates. To evaluate this aspect, we monitored fluorescence recovery after photobleaching (FRAP) in large PAB-1 and TIAR-2 puncta (Figures 3E–3I). All large TIAR-2 puncta and half of the large PAB-1 puncta in aged animals showed no fluorescence recovery, demonstrating that these are solid aggregates (Figures 3E–3I). Because of the small size of the age-dependent stress-granule-like puncta, it was not possible to assess the mobility of TIAR-2 or PAB-1 in these structures. Consequently, we used the large puncta as a readout for sgRBP aggregation in subsequent experiments.

Aggregation of Key Stress Granule Component PAB-1 Is Associated with Reduced Fitness

The consequences of age-dependent protein aggregation for the animal's health are poorly understood. Here, we evaluated the impact of the aggregation of a key stress granule component during aging. Surprisingly, PAB-1 overexpression was protective as animals, grown at 15°C, 20°C, or 25°C all their life, lived longer than non-transgenic animals (Table S5). However, this effect is likely due to higher levels of functional PAB-1 and not related to protein aggregation because PAB-1 does not aggregate in animals at 15°C (Figure S5A). In order to distinguish effects specifically related to PAB-1 aggregation, we separated PAB-1 transgenics at day 7 into three groups depending on their aggregation levels. We found that animals with PAB-1 aggregation were significantly smaller in size compared with animals without PAB-1 aggregation (Figure 4A; Figure S5B). In addition, smaller animals were visibly less motile (Movie S1). Importantly, mildly stressed animals with the highest levels of aggregation died earlier (Figure 4B; Table S5). Overall, these results demonstrate that PAB-1 aggregation is associated with impaired health.

HSF-1 Activity during Development Protects against sgRBP Aggregation

Our proteomic study revealed that reduced *daf-2* signaling efficiently prevents the insolubility of stress granule components with age. We confirmed that long-lived *daf-2* mutants greatly delay the formation of both stress-granule-like structures and large aggregates of PAB-1 and TIAR-2 (Figures 5A and 5B; Figures S6A and S6B). To gain insight into the mechanisms controlling protein aggregation, we investigated the role of the transcription factor HSF-1 activated by reduced *daf-2* signaling (Hsu et al., 2003; Volovik et al., 2012). Chaperones HSP110, HSP70, and HSP40 modulate stress granule dynamics in *Saccharomyces cerevisiae* and/or in cell culture (Cherkasov et al., 2013; Gilks et al., 2004; Kroschwald et al., 2015; Walters et al., 2015). Because chaperone expression is controlled by HSF-1 in *C. elegans*, we speculated that HSF-1 may regulate sgRBP aggregation. Indeed, impairing HSF-1 activity in both *daf-2(−)* and wild-type backgrounds caused severe PAB-1 aggregation already in young adults as well as in aged individuals, an effect that was reversed by overexpressing HSF-1 (Figures 5C–5E; Figures S6C and S6D). Interestingly, HSF-1 in *daf-2* mutants did not control the aggregation of the kinase KIN-19, which was previously shown to misfold and form solid aggregates with age (Figure 5G) (David et al., 2010). These results suggest that HSF-1 regulates different types of endogenous protein aggregation with age to different extents. It was previously shown that to assure *daf-2(−)* longevity, HSF-1 is most highly expressed and acts mainly during development (Volovik et al., 2012). We observed that impairing HSF-1 activity by RNAi during adulthood had no effect on PAB-1 aggregation (Figure 5F; Figure S6E). Conversely, reducing HSF-1 activity by RNAi during development caused PAB-1 aggregation in young adults, albeit mainly in the anterior bulb (Figure 5F).

Figure 3. TIAR-2 and PAB-1 Accumulate in Stress-Granule-like Puncta and Large Immobile Puncta in Aged *C. elegans*

(A) Small Venus::TIAR-2 puncta formed with age are similar to stress granules formed during heat stress. Representative single-plane images and masks of puncta for size quantification. Scale bars, 5 μm.

(B) Size quantification of Venus::TIAR-2 puncta from masks of representative single-plane images in (A).

(C) Representative single-plane images and masks of puncta for size quantification showing large tagRFP::PAB-1 puncta formed with age compared with stress granules assembled during heat stress. Scale bars, 5 μm.

(D) Size quantification of tagRFP::PAB-1 puncta from masks of representative single-plane images in (C). Puncta larger than 0.5 μm^2 were considered as "large" puncta.

(E) Representative immobile tagRFP::PAB-1 puncta at day 11 assayed by FRAP. Bleached area is marked by white box. Scale bar, 4 μm.

(F) Representative immobile Venus::TIAR-2 puncta at day 8 assayed by FRAP. Bleached area is marked by white box. Scale bar, 2 μm.

(G) FRAP analysis of immobile tagRFP::PAB-1 puncta present in aged worms (days 11–12). Quantification of relative fluorescence intensity (RFI) over time. Number of animals = 6, puncta evaluated = 6, mean ± SD is represented.

(H) Venus::TIAR-2 puncta monitored by FRAP were highly immobile both in young (day 2) and in aged (day 8) animals. In both young and aged animals: animals = 5, puncta evaluated = 5, mean ± SD is represented.

(I) Quantification of FRAP results shows increased immobility of tagRFP::PAB-1 puncta with age. Twenty percent of tagRFP::PAB-1 puncta present in young worms (day 2) were immobile (number of animals = 18, puncta evaluated = 57) compared with 51% in aged worms (days 11–15) (number of animals = 18, puncta evaluated = 55).

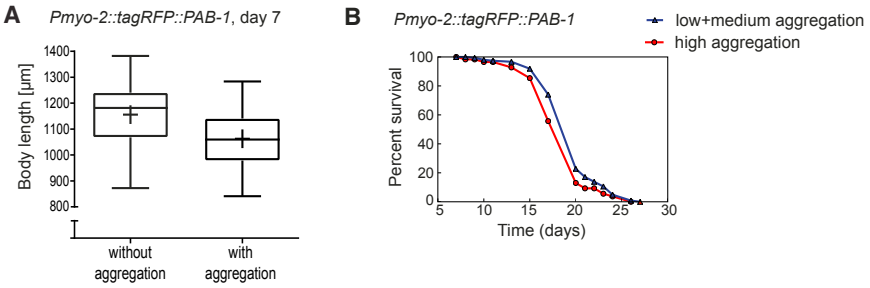

Figure 4. Aggregation of Stress Granule Component PAB-1 with Age Is Associated with Reduced Fitness

(A) Animals with tagRFP::PAB-1 aggregation are significantly smaller than animals without aggregation (day 7, $p < 0.0001$). Data are represented with Tukey-style box plots and mean indicated by + (animals without aggregation n = 99, with aggregation n = 125). See also Figure S5B.

(B) High levels of tagRFP::PAB-1 aggregation are associated with reduced survival. Survival curve of *Pmyo-2::tagRFP::PAB-1* animals grown at 20°C until day 7, sorted by their aggregation levels at day 7, and then transferred to 25°C (repeat 1: $p = 0.029$; see Table S5).

See also Figure S5, Table S5, and Movie S1.

The same chaperones discovered to regulate stress granule dynamics in other model systems could also play a role in preventing sgRBP aggregation. In yeast the Hsp40 proteins Sis1 and Ydj1 were shown to co-localize with stress granules and to play a role in stress granule disassembly (Walters et al., 2015). We evaluated worm strains overexpressing yellow fluorescent protein (YFP)-tagged DNJ-13 and DNJ-19, the worm orthologs of Sis1 and Ydj1, together with tagRFP::PAB-1. We observed occasional co-localization of both chaperones with both heat-induced PAB-1 stress granules and age-dependent large and stress-granule-like PAB-1 puncta (Figures S6G and S6H). These findings were confirmed in single tagRFP::PAB-1 transgenics using antibodies against DNJ-13 and DNJ-19 (data not shown). However, overexpression of DNJ-19 and DNJ-13 did not significantly reduce PAB-1 aggregation with age (Figures S6F and S6I), indicating that these chaperones may not modulate sgRBP aggregation. In addition, we performed immunostaining for HSP110. However, we observed no co-staining with either PAB-1 stress granules induced by heat shock or PAB-1 puncta formed during aging. Therefore, it is possible that HSP110 does not modulate stress granule dynamics and sgRBP aggregation in *C. elegans*. Finally, we investigated the role of HSP70 on sgRBP aggregation and found that inhibition of HSP70 by RNAi did not alter PAB-1 aggregation (Table S6). Of note, the later results could be caused by redundancy between chaperone functions.

Collectively, these results reveal that HSF-1 is an important regulator of sgRBP aggregation throughout life, and it contributes to maintaining dynamic stress granule proteins in long-lived *daf-2* mutants. The exact chaperones responsible for preventing sgRBP aggregation remain to be determined.

daf-2 Mutants Avoid sgRBP Aggregation in Part by Eliminating Putative Cross-Seeding

Next, we examined the role of the transcription factor DAF-16 activated by reduced *daf-2* signaling (Lin et al., 1997; Ogg et al., 1997). In *daf-2* mutants, DAF-16 protected against PAB-1 aggregation in aged animals (Figures 5C and 5D). Importantly, *daf-2* mutants use DAF-16 to control different types of age-dependent protein aggregation because delayed aggregation of the kinase KIN-19 was also dependent on DAF-16 (Figure 5G).

Recent work performed in *S. cerevisiae* and *Drosophila* reveals that stress granules dynamically interact with misfolded proteins (Cherkasov et al., 2013; Kroschwald et al., 2015). We speculated that widespread protein misfolding and aggregation occurring with age could promote sgRBP aggregation. In support of this hypothesis, we observed the co-localization of PAB-1 and KIN-19 in large immobile aggregates in double transgenics (Figures 6A and 6B). Next, we evaluated the rate of PAB-1 and KIN-19 aggregation in the double transgenics relative to their aggregation rates in single transgenics (Figures 6C and 6D). In the single transgenics, KIN-19 aggregated faster and to a greater extent than PAB-1. Importantly, when both PAB-1 and KIN-19 were co-expressed, the presence of misfolded KIN-19 triggered more abundant PAB-1 aggregation at an earlier age (Figure 6C). Conversely, KIN-19 aggregation was slightly impeded by PAB-1 overexpression (Figure 6D), indicating that sgRBP aggregation does not cross-seed KIN-19 aggregation. Notably, PAB-1 aggregation was not accelerated by the co-expression of a fluorescent tag alone (Figure 6E). Furthermore, we did not observe a general induction of PAB-1 stress granules in young double-transgenic animals expressing both KIN-19 and PAB-1 (Figure S6J). These data strongly suggest that PAB-1 aggregation is not simply the consequence of generalized cellular stress induced by KIN-19 overexpression. Rather, the co-localization of KIN-19 and PAB-1 in the same aggregates as well as the earlier and accelerated aggregation of PAB-1 is consistent with a seeding mechanism related to KIN-19 aggregation.

Taken together, we interpret these findings to imply that the accumulation of misfolded proteins with age acts as a seed for sgRBP aggregation. Therefore, the overall reduction in widespread protein aggregation in long-lived *daf-2(–)* conditions as evidenced by our proteomic analysis, at least in part through increased DAF-16 activity, could be an effective strategy to prevent sgRBP aggregation.

Other Longevity Pathways Prevent Age-Dependent sgRBP Aggregation

Several experimental manipulations have been shown to extend the lifespan of *C. elegans* and protect against proteotoxicity (Kenyon, 2010; Taylor and Dillin, 2011). We wondered whether other pathways extending lifespan could also protect against sgRBP aggregation. We found that both dietary restriction mimicked in *eat-2* mutant animals as well as inhibition of mitochondrial function achieved by targeting *cyc-1* with RNAi strongly limited PAB-1 aggregation with age (Figures 7A and

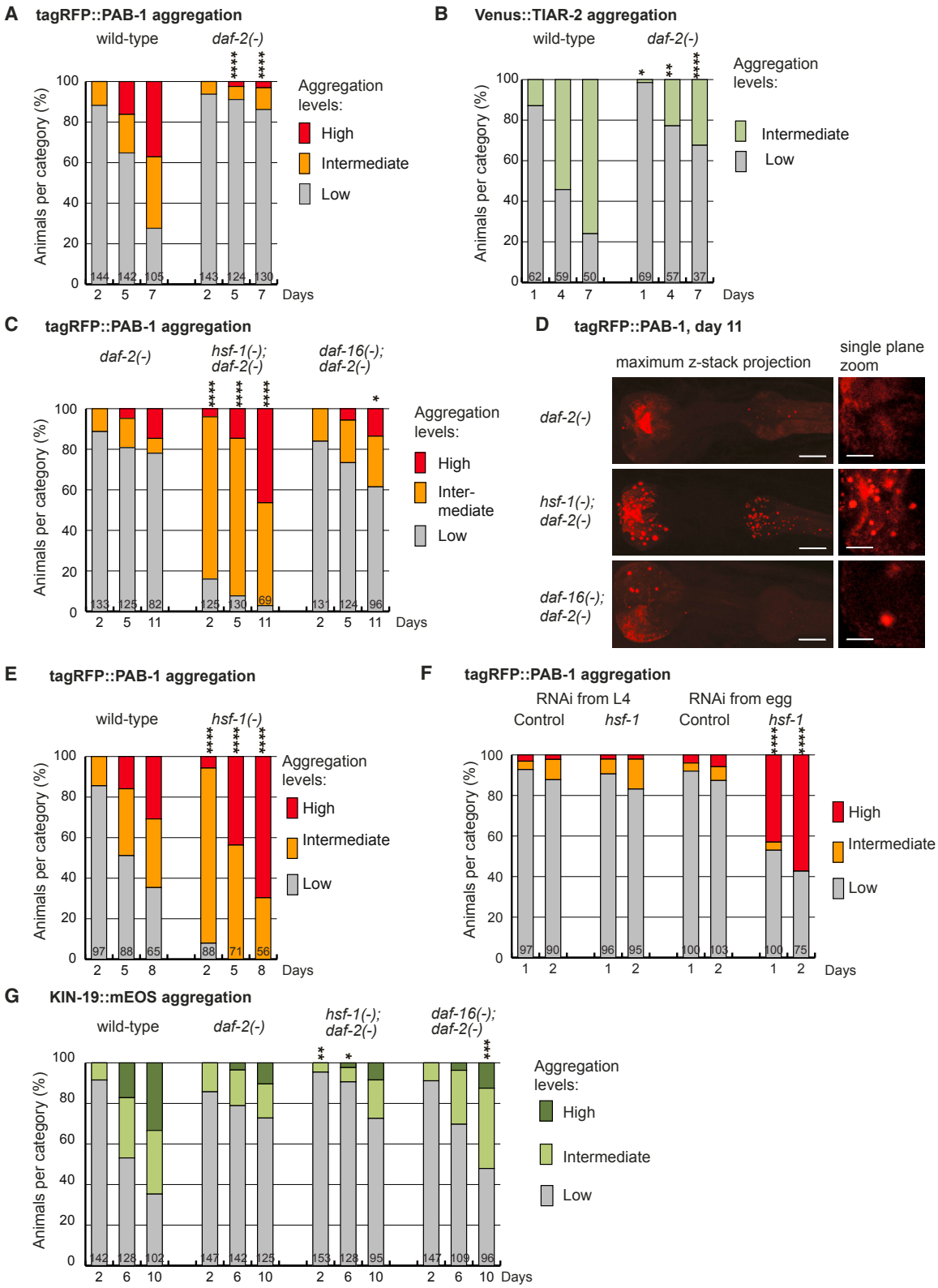

(legend on next page)

7B). Therefore, maintaining dynamic RBPs could be a common strategy associated with longevity.

DISCUSSION

We show that a wide variety of RNA granule components become highly insoluble with age in *C. elegans*. Together with previous in vitro and cell culture results, our findings demonstrate that the capacity of RBPs to cycle between assembled and disassembled states can become a liability in aging organisms. Already in young animals, maintaining sgRBP dynamics necessitates an active control system established by HSF-1. The accumulation of other misfolded proteins during age acts as a seed for the aggregation of key sgRBPs. Significantly, one of the main outcomes of the longevity program initiated by reduced *daf-2* signaling while responding to widespread protein aggregation is the preservation of RBP solubility with age.

In this study, we have examined in detail the aggregation pattern of PAB-1 and TIAR-2, two key RBPs with LC prion-like domains that are important for the formation of stress granules. During the aging process, both proteins spontaneously assembled into small puncta similar to liquid droplets induced during stress and into larger aggregates. Significantly, upon co-expression, both PAB-1 and TIAR-2 co-localized in these age-related stress-granule-like structures. Because our proteomic analysis revealed a number of stress granule components in the insoluble proteome, it is likely that secondary stress granule proteins are also incorporated. Therefore, an attractive hypothesis is that these small puncta represent stress granules formed as a response to stress related to aging. The inherent aggregation propensity of sgRBPs would induce at least some of these droplets to undergo the irreversible transition into a solid state. These stabilized stress granules could then grow into large aggregates as we observed with PAB-1, or simply accumulate with age as seen with TIAR-2.

An important question remains how the inherent propensity of RNA granule components to aggregate with age could influence pathogenesis in neurodegenerative diseases.

One possibility is that inherent RBP aggregation impacts cellular health and thereby indirectly accelerates pathology. We observed reduced lifespan and a striking decrease in size and mobility of animals with higher levels of PAB-1 aggregation. As yet, it remains unclear whether reduced fitness is a cause or consequence of PAB-1 aggregation. In support of a gain of function related to sgRBP aggregation, two rare diseases are caused by mutated PABPN1 and TIA-1, the human homologs of PAB-1 and TIAR-2, which accumulate in pathological aggregates (Brais et al., 1998; Klar et al., 2013). Our proteomic analysis of aging *C. elegans* highlighted three other RBPs with LC prion-like domains that are highly prone to aggregate with age: HRP-1, FIB-1, and CAR-1. The aggregation of the human homologs of HRP-1, hnRNP-A1, and hnRNP-A3 was recently discovered to cause multisystem proteinopathy and ALS/FTLD (Kim et al., 2013; Mori et al., 2013). The aggregation of both FIB-1 and CAR-1 could also be detrimental. Indeed, a loss in nucleolar protein FIB-1 function caused by its aggregation with age could impair ribosomal biogenesis (Tollervey et al., 1991). The mammalian LSM14B and LSM14A homologs of CAR-1 localize to P bodies (Eulalio et al., 2007), and aggregation of key P-body components could impair non-sense-mediated decay. Therefore, it will be important to investigate the consequences of FIB-1 and CAR-1 aggregation on cellular health.

Apart from accelerating pathology indirectly by reducing cellular health, aggregating RBPs could directly influence pathological protein aggregation. The presence of stress granule proteins in pathological protein aggregates is emerging as a common denominator in different types of neurodegenerative diseases including ALS, FTLD, Alzheimer's disease, and Huntington's disease (Aulas and Vande Velde, 2015; Bentmann et al., 2013). The inherent aggregation propensity of stress granule proteins demonstrates that they are unlikely to be transient interacting partners in pathological aggregates. It remains to be determined whether age-related sgRBP aggregation acts as a seed for disease-associated protein aggregation. Overall, the role of stress granules in neurodegenerative diseases is clearly highly complex because there is evidence supporting the recruitment of disease-associated proteins to stress granules and vice versa. Interestingly, recent cell culture data show that the assembly of stress granules caused by disease-associated protein aggregation in turn promotes pathological aggregation (Vanderweyde et al., 2016).

The age-dependent aggregation of sgRBPs and prevalence of stress granule components in neurodegenerative diseases underline their relevance as therapeutic targets. One successful strategy would be to prevent the initial assembly of stress granules (Kim et al., 2014). Our work suggests another possibility,

Figure 5. HSF-1 Activity during Development Protects against PAB-1 Aggregation in Adulthood in *daf-2* Mutant and Wild-Type Adults

(A) Delayed tagRFP::PAB-1 aggregation with age in *daf-2* mutant background. Days 5 and 7, *daf-2(–)* versus wild-type background: ****p < 0.0001.

(B) Delayed Venus::TIAR-2 aggregation with age in *daf-2* mutant background. Days 1, 4 and 7, *daf-2(–)* versus wild-type background: *p < 0.05, **p < 0.01, and ****p < 0.0001, respectively.

(C) Levels of tagRFP::PAB-1 aggregation are highly increased at all ages examined in *hsf-1(–); daf-2(–)* animals compared with *daf-2(–)* animals. DAF-16 moderately protects against tagRFP::PAB-1 aggregation at day 11. *daf-2(–)* compared with *hsf-1(–);daf-2(–)*: ****p < 0.0001; *daf-2(–)* compared with *daf-16(–);daf-2(–)*: *p = 0.02.

(D) Head regions of representative animals expressing *Pmyo-2::tagRFP::PAB-1* in *daf-2(–), hsf-1(–); daf-2 (–)* and *daf-16(–); daf-2(–)* mutants at day 11. Scale bars: z stack projection, 15 μm; single-plane zoom, 5 μm.

(E) *hsf-1* mutation alone increases tagRFP::PAB-1 aggregation dramatically, even at day 2. ****p < 0.0001.

(F) HSF-1 activity during development is essential in order to delay tagRFP::PAB-1 aggregation (control: L4440 empty vector). Days 1 and 2 with RNAi treatment from egg, ****p < 0.0001.

(G) Delayed KIN-19::mEOS (monomeric EOS) aggregation with age in *daf-2* mutants is dependent on DAF-16, but not on HSF-1. *daf-2(–)* compared with *hsf-1(–); daf-2(–)*: day 2, **p = 0.0049; day 6, *p = 0.01. *daf-2(–)* compared with *daf-16(–);daf-2(–)*: ***p = 0.0003, day 10.

See also Figure S6 and Table S6.

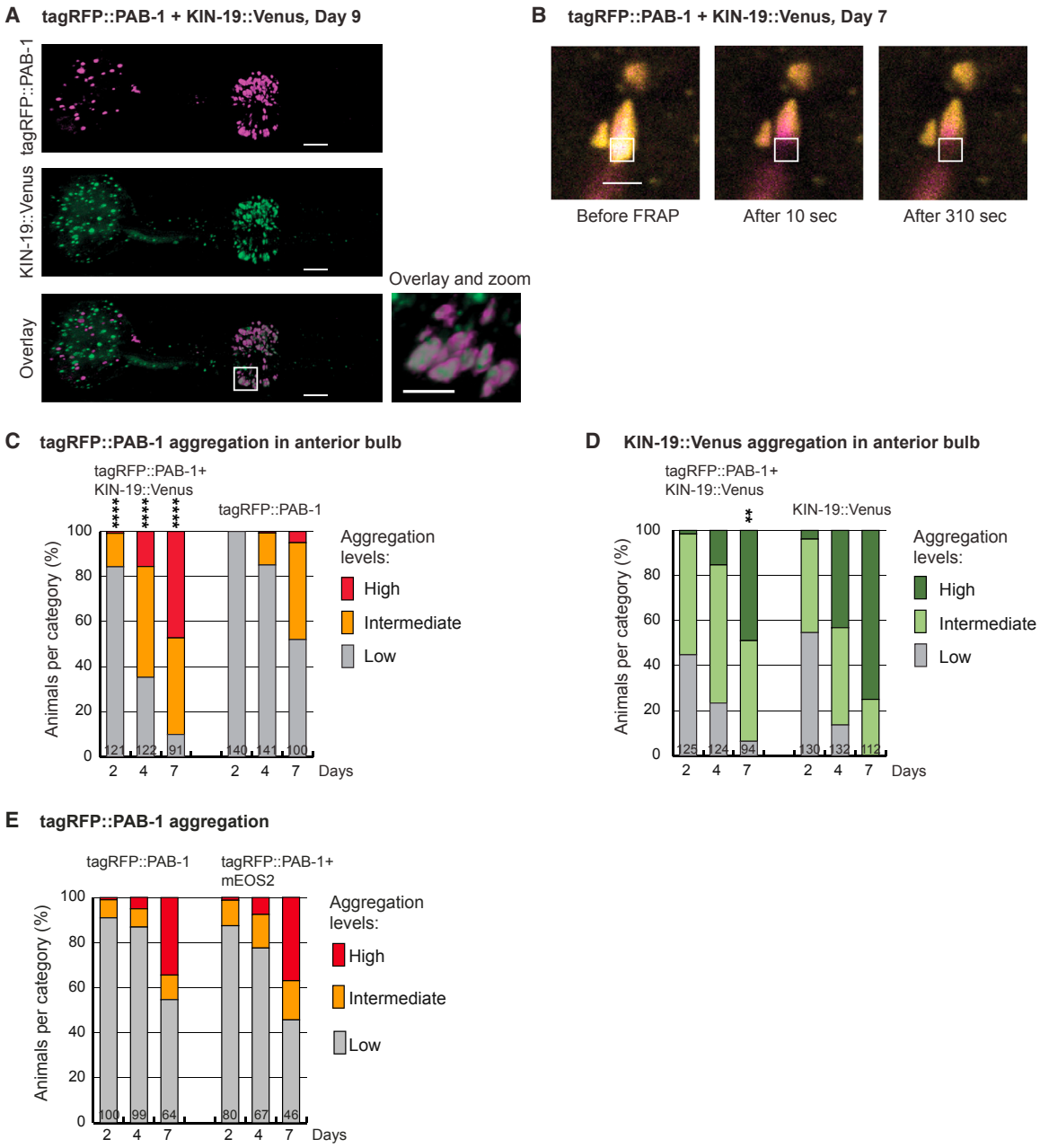

Figure 6. PAB-1 Aggregation Is Accelerated by KIN-19

(A) tagRFP::PAB-1 co-localizes with KIN-19::Venus in large aggregates in double-transgenic animals. Representative head region displayed in 3D. Scale bars, 10 μm; overlay and zoom scale bar, 5 μm.

(B) Representative immobile mixed tagRFP::PAB-1 (magenta) and KIN-19::Venus (yellow) puncta at day 7 assayed by FRAP. Bleached area is marked by white box. Scale bar, 2 μm.

(C) Accelerated tagRFP::PAB-1 aggregation in the anterior pharyngeal bulb in double transgenics compared with single transgenics. Days 2, 4, and 7: ****$p < 0.0001$.

(D) Moderately reduced KIN-19::Venus aggregation in the anterior pharyngeal bulb in double transgenics compared with single transgenics. Day 7: **$p = 0.0083$.

(E) No significant increase of tagRFP::PAB-1 aggregation in the presence of mEOS2 overexpression. At all ages, $p > 0.05$.

See also Figure S6.

namely abrogating sgRBP aggregation. In future work, it will be important to understand how longevity pathways relying on dietary restriction or defective mitochondrial respiration efficiently prevent sgRBP aggregation. In the case of reduced *daf-2* signaling, sgRBP aggregation is suppressed by at least two mechanisms: DAF-16 activation prevents cross-seeding by

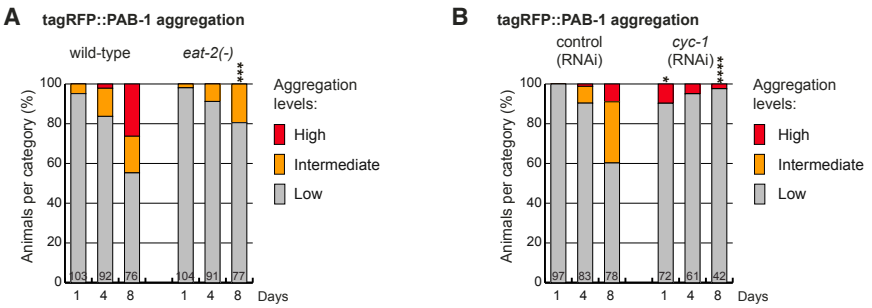

Figure 7. Other Longevity Pathways Prevent PAB-1 Aggregation with Age

(A) Dietary restriction delays tagRFP::PAB-1 aggregation with age. Day 8, *eat-2(–)* versus wild-type background: ***p < 0.001.

(B) Inhibition of mitochondrial function by *cyc-1* RNAi halts tagRFP::PAB-1 aggregation. Days 1 and 8, *cyc-1* RNAi versus control: *p < 0.05 and ****p < 0.0001, respectively.

delaying the accumulation of misfolded aggregation-prone proteins, and increased activity of HSF-1 during development assures enhanced sgRBP proteostasis throughout adulthood. To date, cross-seeding of RBP aggregation has been observed only with the Huntingtin protein containing an expanded polyglutamine repeat region (Furukawa et al., 2009). It will be important to investigate by which means endogenous aggregation-prone proteins lacking motifs similar to the LC prion-like domain would cross-seed RBPs aggregation. Overall, both of these strategies used to restore the dynamic nature of stress granule proteins could also directly prevent disease-associated RBP aggregation.

EXPERIMENTAL PROCEDURES

A list of strains, strain maintenance, RNAi treatment, and lifespan assays is described in the Supplemental Experimental Procedures.

Heat Shock

Nematodes were heat shocked in M9 medium with OP50 on a nutator. Control worms were treated the same at 20°C. Worms were either fixed for imaging analysis directly after heat shock or allowed to recover on normal growth (NG) plates kept at 20°C before fixation.

Size Measurements

Images were taken of synchronized live *C. elegans* using a Leica fluorescence microscope M165 FC with a Planapo 2.0× objective and Leica DFC310 FX camera. Body length was determined for each worm using Fiji software (Schindelin et al., 2012). Significance was evaluated by unpaired, two-tailed t test using GraphPad Prism 6.

Imaging and Immunofluorescence Staining

Worms were examined with a Leica SP8 confocal microscope. Fixation and immunostaining protocol including imaging parameters are described in the Supplemental Experimental Procedures. Representative confocal images are displayed as maximum z stack projection unless mentioned otherwise.

Aggregation Quantification In Vivo

In a population of synchronized live *C. elegans*, aggregation levels were determined using a Leica fluorescence microscope M165 FC with a Planapo 2.0× objective. Animals overexpressing *Pmyo-2::Venus::TIAR-2* were divided into two categories: animals with up to 10 (low aggregation) or more than 10 Venus::TIAR-2 puncta (intermediate aggregation) in the anterior and posterior pharyngeal bulb. Animals overexpressing *Pmyo-2:tagRFP:PAB-1* were divided into three categories: animals with up to 10 (low aggregation) or more than 10 (intermediate aggregation) tagRFP::PAB-1 puncta in the posterior bulb, or more than 10 (high aggregation) tagRFP:PAB-1 puncta in the anterior bulb. The latter mostly had more than 10 puncta in the posterior bulb. Animals expressing *Pkin-19::KIN-19::mEOS* or *Pkin-19::KIN-19::Venus* were divided into less than 10 puncta (low aggregation), between 10 and 100 puncta (intermediate aggregation), and more than 100 puncta in the anterior bulb (high aggregation). To compare aggregation levels between KIN-19::Venus and tagRFP::PAB-1, we evaluated tagRFP::PAB-1 puncta formation only in the anterior bulb and with the same counting scheme as for KIN-19::Venus. When comparing different strains, counting was done in a blind fashion. For statistics, two-tailed Fisher's exact test was performed using an online tool (http://www.socscistatistics.com/tests/fisher/default2.aspx). Significance of high + intermediate against low aggregation levels was calculated unless indicated otherwise. Numbers of animals per time point are indicated in the graphic bars.

FRAP Analysis

FRAP analysis was performed as previously described (David et al., 2010) using the Leica SP8 confocal microscope with the harmonic compound, plan, apochromatic (HC PL APO) CS2 63× 1.30 glycerol objective and photomultiplier tube (PMT) detector. Further experimental details are described in the Supplemental Experimental Procedures.

Insoluble Protein Extraction, Quantification, and Mass Spectrometry Analysis

To obtain large synchronized populations of aged animals and quantify protein aggregation only in the somatic tissues, we used temperature-induced sterile *gon-2* mutants as previously described (David et al., 2010). To induce longevity, we subjected animals to *daf-2* RNAi and control animals to *gfp* RNAi from the last larval stage L4 onward. Animals aged at 25°C were collected at day 3 of adulthood (young) and when half the control animals had died between days 14 and 18 (aged). No significant death was observed in long-lived animals on *daf-2* RNAi. Isolation of large SDS insoluble aggregates for immunoblot and mass spectrometry analysis were performed as previously described (David et al., 2010). See Supplemental Experimental Procedures for further details and antibodies used for immunoblots. The mass spectrometry proteomics data have been deposited to the ProteomeXchange Consortium (http://proteomecentral.proteomexchange.org) via the PRIDE partner repository (Vizcaíno et al., 2014) with the dataset identifier PXD003451.

Bioinformatics Analysis

Aliphatic amino acid residues were defined as A, G, I, L, and V. Secondary structure content was predicted using PSIPRED v2.6 (Jones, 1999). The p values were calculated using the unequal variance t test compared with the background set of all proteins detected by mass spectrometry (n = 5,637). Additional details and functional analysis are described in the Supplemental Experimental Procedures.

ACCESSION NUMBERS

The accession number for the mass spectrometry proteomics data reported in this paper is PRIDE: PXD003451.

SUPPLEMENTAL INFORMATION

Supplemental Information includes Supplemental Experimental Procedures, six figures, six tables, and one movie and can be found with this article online at http://dx.doi.org/10.1016/j.celrep.2016.12.033.

AUTHOR CONTRIBUTIONS

M.C.L., N.G., J.C.T., and D.C.D. designed and performed experiments. E.D.C. performed bioinformatics analysis. K.W., R.J., and J.K. generated reagents. J.K. performed chaperone immunostainings. A.L.B. provided analytical tools, reagents, and materials. M.C.L., J.C.T., and D.C.D. wrote the paper.

ACKNOWLEDGMENTS

We are grateful to Cynthia Kenyon for help in the early stages of this project. We thank Aimee Kao and Sivan Henis-Korenblit for critical input, David Maltby for mass spectrometry support, Aenoch Lynn for help with the proteomic data analysis, Brian Lee for basic gateway constructs, and Kristin Arnsburg for integrating DNJ-13 and DNJ-19 transgenics. We are grateful to Simon Alberti for sharing the *C. elegans* list of proteins with prion-like domains. For the generous donation of antibodies, we would like to thank Rafal Ciosk (anti-PAB-1), Junho Lee (anti-HRP-1), and Keith Blackwell (anti-CAR-1). The *gon-2* mutants were kindly provided by Eric Lambie. This work was initiated in Cynthia Kenyon's lab and was funded by an Ellison/AFAR postdoctoral fellowship (to D.C.D.) and by the NIH (NIGMS grant 8P41GM103481 to A.L.B. and grant P50 GM081879 to J.C.T. and A.L.B.). Subsequently, this work was supported by funding from the DZNE and a Marie Curie International Reintegration Grant (322120 to D.C.D.).

Received: August 11, 2016
Revised: October 28, 2016
Accepted: December 12, 2016
Published: January 10, 2017

REFERENCES

Alberti, S., Halfmann, R., King, O., Kapila, A., and Lindquist, S. (2009). A systematic survey identifies prions and illuminates sequence features of prionogenic proteins. Cell *137*, 146–158.

Arai, T., Hasegawa, M., Akiyama, H., Ikeda, K., Nonaka, T., Mori, H., Mann, D., Tsuchiya, K., Yoshida, M., Hashizume, Y., and Oda, T. (2006). TDP-43 is a component of ubiquitin-positive tau-negative inclusions in frontotemporal lobar degeneration and amyotrophic lateral sclerosis. Biochem. Biophys. Res. Commun. *351*, 602–611.

Aulas, A., and Vande Velde, C. (2015). Alterations in stress granule dynamics driven by TDP-43 and FUS: a link to pathological inclusions in ALS? Front. Cell. Neurosci. *9*, 423.

Ayyadevara, S., Mercanti, F., Wang, X., Mackintosh, S.G., Tackett, A.J., Prayaga, S.V., Romeo, F., Shmookler Reis, R.J., and Mehta, J.L. (2016). Age- and hypertension-associated protein aggregates in mouse heart have similar proteomic profiles. Hypertension *67*, 1006–1013.

Balch, W.E., Morimoto, R.I., Dillin, A., and Kelly, J.W. (2008). Adapting proteostasis for disease intervention. Science *319*, 916–919.

Bentmann, E., Neumann, M., Tahirovic, S., Rodde, R., Dormann, D., and Haass, C. (2012). Requirements for stress granule recruitment of fused in sarcoma (FUS) and TAR DNA-binding protein of 43 kDa (TDP-43). J. Biol. Chem. *287*, 23079–23094.

Bentmann, E., Haass, C., and Dormann, D. (2013). Stress granules in neurodegeneration–lessons learnt from TAR DNA binding protein of 43 kDa and fused in sarcoma. FEBS J. *280*, 4348–4370.

Brais, B., Bouchard, J.P., Xie, Y.G., Rochefort, D.L., Chrétien, N., Tomé, F.M., Lafrenière, R.G., Rommens, J.M., Uyama, E., Nohira, O., et al. (1998). Short GCG expansions in the PABP2 gene cause oculopharyngeal muscular dystrophy. Nat. Genet. *18*, 164–167.

Cherkasov, V., Hofmann, S., Druffel-Augustin, S., Mogk, A., Tyedmers, J., Stoecklin, G., and Bukau, B. (2013). Coordination of translational control and protein homeostasis during severe heat stress. Curr. Biol. *23*, 2452–2462.

David, D.C. (2012). Aging and the aggregating proteome. Front. Genet. *3*, 247.

David, D.C., Ollikainen, N., Trinidad, J.C., Cary, M.P., Burlingame, A.L., and Kenyon, C. (2010). Widespread protein aggregation as an inherent part of aging in C. elegans. PLoS Biol. *8*, e1000450.

Demontis, F., and Perrimon, N. (2010). FOXO/4E-BP signaling in Drosophila muscles regulates organism-wide proteostasis during aging. Cell *143*, 813–825.

Eulalio, A., Behm-Ansmant, I., and Izaurralde, E. (2007). P bodies: at the crossroads of post-transcriptional pathways. Nat. Rev. Mol. Cell Biol. *8*, 9–22.

Furukawa, Y., Kaneko, K., Matsumoto, G., Kurosawa, M., and Nukina, N. (2009). Cross-seeding fibrillation of Q/N-rich proteins offers new pathomechanism of polyglutamine diseases. J. Neurosci. *29*, 5153–5162.

Gilks, N., Kedersha, N., Ayodele, M., Shen, L., Stoecklin, G., Dember, L.M., and Anderson, P. (2004). Stress granule assembly is mediated by prion-like aggregation of TIA-1. Mol. Biol. Cell *15*, 5383–5398.

Goudeau, J., and Aguilaniu, H. (2010). Carbonylated proteins are eliminated during reproduction in C. elegans. Aging Cell *9*, 991–1003.

Han, T.W., Kato, M., Xie, S., Wu, L.C., Mirzaei, H., Pei, J., Chen, M., Xie, Y., Allen, J., Xiao, G., and McKnight, S.L. (2012). Cell-free formation of RNA granules: bound RNAs identify features and components of cellular assemblies. Cell *149*, 768–779.

Hsu, A.L., Murphy, C.T., and Kenyon, C. (2003). Regulation of aging and age-related disease by DAF-16 and heat-shock factor. Science *300*, 1142–1145.

Johnson, B.S., Snead, D., Lee, J.J., McCaffery, J.M., Shorter, J., and Gitler, A.D. (2009). TDP-43 is intrinsically aggregation-prone, and amyotrophic lateral sclerosis-linked mutations accelerate aggregation and increase toxicity. J. Biol. Chem. *284*, 20329–20339.

Jones, D.T. (1999). Protein secondary structure prediction based on position-specific scoring matrices. J. Mol. Biol. *292*, 195–202.

Kato, M., Han, T.W., Xie, S., Shi, K., Du, X., Wu, L.C., Mirzaei, H., Goldsmith, E.J., Longgood, J., Pei, J., et al. (2012). Cell-free formation of RNA granules: low complexity sequence domains form dynamic fibers within hydrogels. Cell *149*, 753–767.

Kenyon, C.J. (2010). The genetics of ageing. Nature *464*, 504–512.

Kim, H.J., Kim, N.C., Wang, Y.D., Scarborough, E.A., Moore, J., Diaz, Z., MacLea, K.S., Freibaum, B., Li, S., Molliex, A., et al. (2013). Mutations in prion-like domains in hnRNPA2B1 and hnRNPA1 cause multisystem proteinopathy and ALS. Nature *495*, 467–473.

Kim, H.J., Raphael, A.R., LaDow, E.S., McGurk, L., Weber, R.A., Trojanowski, J.Q., Lee, V.M., Finkbeiner, S., Gitler, A.D., and Bonini, N.M. (2014). Therapeutic modulation of eIF2α phosphorylation rescues TDP-43 toxicity in amyotrophic lateral sclerosis disease models. Nat. Genet. *46*, 152–160.

King, O.D., Gitler, A.D., and Shorter, J. (2012). The tip of the iceberg: RNA-binding proteins with prion-like domains in neurodegenerative disease. Brain Res. *1462*, 61–80.

Klar, J., Sobol, M., Melberg, A., Mäbert, K., Ameur, A., Johansson, A.C., Feuk, L., Entesarian, M., Orlén, H., Casar-Borota, O., and Dahl, N. (2013). Welander distal myopathy caused by an ancient founder mutation in TIA1 associated with perturbed splicing. Hum. Mutat. *34*, 572–577.

Kroschwald, S., Maharana, S., Mateju, D., Malinovska, L., Nüske, E., Poser, I., Richter, D., and Alberti, S. (2015). Promiscuous interactions and protein disaggregases determine the material state of stress-inducible RNP granules. eLife *4*, e06807.

Li, Y.R., King, O.D., Shorter, J., and Gitler, A.D. (2013). Stress granules as crucibles of ALS pathogenesis. J. Cell Biol. *201*, 361–372.

Lin, K., Dorman, J.B., Rodan, A., and Kenyon, C. (1997). daf-16: an HNF-3/forkhead family member that can function to double the life-span of Caenorhabditis elegans. Science *278*, 1319–1322.

Lin, Y., Protter, D.S., Rosen, M.K., and Parker, R. (2015). Formation and maturation of phase-separated liquid droplets by RNA-binding proteins. Mol. Cell *60*, 208–219.

Molliex, A., Temirov, J., Lee, J., Coughlin, M., Kanagaraj, A.P., Kim, H.J., Mittag, T., and Taylor, J.P. (2015). Phase separation by low complexity domains

promotes stress granule assembly and drives pathological fibrillization. Cell *163*, 123–133.

Mori, K., Lammich, S., Mackenzie, I.R., Forné, I., Zilow, S., Kretzschmar, H., Edbauer, D., Janssens, J., Kleinberger, G., Cruts, M., et al. (2013). hnRNP A3 binds to GGGGCC repeats and is a constituent of p62-positive/TDP43-negative inclusions in the hippocampus of patients with C9orf72 mutations. Acta Neuropathol. *125*, 413–423.

Murakami, T., Yang, S.P., Xie, L., Kawano, T., Fu, D., Mukai, A., Bohm, C., Chen, F., Robertson, J., Suzuki, H., et al. (2012). ALS mutations in FUS cause neuronal dysfunction and death in Caenorhabditis elegans by a dominant gain-of-function mechanism. Hum. Mol. Genet. *21*, 1–9.

Murakami, T., Qamar, S., Lin, J.Q., Schierle, G.S., Rees, E., Miyashita, A., Costa, A.R., Dodd, R.B., Chan, F.T., Michel, C.H., et al. (2015). ALS/FTD mutation-induced phase transition of FUS liquid droplets and reversible hydrogels into irreversible hydrogels impairs RNP granule function. Neuron *88*, 678–690.

Neumann, M., Sampathu, D.M., Kwong, L.K., Truax, A.C., Micsenyi, M.C., Chou, T.T., Bruce, J., Schuck, T., Grossman, M., Clark, C.M., et al. (2006). Ubiquitinated TDP-43 in frontotemporal lobar degeneration and amyotrophic lateral sclerosis. Science *314*, 130–133.

Neumann, M., Rademakers, R., Roeber, S., Baker, M., Kretzschmar, H.A., and Mackenzie, I.R. (2009). A new subtype of frontotemporal lobar degeneration with FUS pathology. Brain *132*, 2922–2931.

Neumann, M., Bentmann, E., Dormann, D., Jawaid, A., DeJesus-Hernandez, M., Ansorge, O., Roeber, S., Kretzschmar, H.A., Munoz, D.G., Kusaka, H., et al. (2011). FET proteins TAF15 and EWS are selective markers that distinguish FTLD with FUS pathology from amyotrophic lateral sclerosis with FUS mutations. Brain *134*, 2595–2609.

Ogg, S., Paradis, S., Gottlieb, S., Patterson, G.I., Lee, L., Tissenbaum, H.A., and Ruvkun, G. (1997). The Fork head transcription factor DAF-16 transduces insulin-like metabolic and longevity signals in C. elegans. Nature *389*, 994–999.

Patel, A., Lee, H.O., Jawerth, L., Maharana, S., Jahnel, M., Hein, M.Y., Stoynov, S., Mahamid, J., Saha, S., Franzmann, T.M., et al. (2015). A liquid-to-solid phase transition of the ALS protein FUS accelerated by disease mutation. Cell *162*, 1066–1077.

Reis-Rodrigues, P., Czerwieniec, G., Peters, T.W., Evani, U.S., Alavez, S., Gaman, E.A., Vantipalli, M., Mooney, S.D., Gibson, B.W., Lithgow, G.J., and Hughes, R.E. (2012). Proteomic analysis of age-dependent changes in protein solubility identifies genes that modulate lifespan. Aging Cell *11*, 120–127.

Rousakis, A., Vlanti, A., Borbolis, F., Roumelioti, F., Kapetanou, M., and Syntichaki, P. (2014). Diverse functions of mRNA metabolism factors in stress defense and aging of Caenorhabditis elegans. PLoS ONE *9*, e103365.

Schindelin, J., Arganda-Carreras, I., Frise, E., Kaynig, V., Longair, M., Pietzsch, T., Preibisch, S., Rueden, C., Saalfeld, S., Schmid, B., et al. (2012). Fiji: an open-source platform for biological-image analysis. Nat. Methods *9*, 676–682.

Tanase, M., Urbanska, A.M., Zolla, V., Clement, C.C., Huang, L., Morozova, K., Follo, C., Goldberg, M., Roda, B., Reschiglian, P., and Santambrogio, L. (2016). Role of carbonyl modifications on aging-associated protein aggregation. Sci. Rep. *6*, 19311.

Taylor, R.C., and Dillin, A. (2011). Aging as an event of proteostasis collapse. Cold Spring Harb. Perspect. Biol. *3*, a004440.

Tollervey, D., Lehtonen, H., Carmo-Fonseca, M., and Hurt, E.C. (1991). The small nucleolar RNP protein NOP1 (fibrillarin) is required for pre-rRNA processing in yeast. EMBO J. *10*, 573–583.

Vanderweyde, T., Apicco, D.J., Youmans-Kidder, K., Ash, P.E., Cook, C., Lummertz da Rocha, E., Jansen-West, K., Frame, A.A., Citro, A., Leszyk, J.D., et al. (2016). Interaction of tau with the RNA-binding protein TIA1 regulates tau pathophysiology and toxicity. Cell Rep. *15*, 1455–1466.

Vizcaíno, J.A., Deutsch, E.W., Wang, R., Csordas, A., Reisinger, F., Ríos, D., Dianes, J.A., Sun, Z., Farrah, T., Bandeira, N., et al. (2014). ProteomeXchange provides globally coordinated proteomics data submission and dissemination. Nat. Biotechnol. *32*, 223–226.

Volovik, Y., Maman, M., Dubnikov, T., Bejerano-Sagie, M., Joyce, D., Kapernick, E.A., Cohen, E., and Dillin, A. (2012). Temporal requirements of heat shock factor-1 for longevity assurance. Aging Cell *11*, 491–499.

Walters, R.W., Muhlrad, D., Garcia, J., and Parker, R. (2015). Differential effects of Ydj1 and Sis1 on Hsp70-mediated clearance of stress granules in Saccharomyces cerevisiae. RNA *21*, 1660–1671.

Walther, D.M., Kasturi, P., Zheng, M., Pinkert, S., Vecchi, G., Ciryam, P., Morimoto, R.I., Dobson, C.M., Vendruscolo, M., Mann, M., and Hartl, F.U. (2015). Widespread proteome remodeling and aggregation in aging C. elegans. Cell *161*, 919–932.

Zimmerman, S.M., Hinkson, I.V., Elias, J.E., and Kim, S.K. (2015). Reproductive aging drives protein accumulation in the uterus and limits lifespan in C. elegans. PLoS Genet. *11*, e1005725.